Postweld Solution Annealing Effects on the Ductility of Ni-Co-Cr-Base Alloy Gas Tungsten Arc Welds

C.-S. Lim and K.-K. Baek

The welding characteristics of a commercial wrought alloy with a nominal composition of Ni-29Co-28Cr-2.75Si were investigated. Gas tungsten arc weldments with filler metal matching the chemistry of the alloy were found to have limited room-temperature ductility in the as-welded condition. Since welding is the main fabrication method of this alloy, the welding and postweld heat treatment (PWHT) characteristics were examined to provide guidelines for fabrication in the field. Metallographic evaluation revealed that the weld metal was characterized by the distribution of a continuous eutectic phase consisting primarily of $(Si,Ti)_xNi_y$. The continuous eutectic phase in the as-welded deposit, which caused poor ductility of the welds, was successfully reduced or removed with proper PWHT. The PWHT is necessary if cold forming of a weldment is required after welding or if adequate joint ductility is a design requirement. The recommended PWHT temperature is 1050 °C.

Keywords
Ni-Co-Cr alloys, postweld heat treatment, tensile properties, welding

1. Introduction

THE DEMAND for more efficient industrial plants has challenged the materials engineering community to develop alloys that can withstand severe service conditions, such as high-temperature, corrosive environments. As a result, the use of high-temperature alloys has increased sharply. For example, Ni-Co-Cr-base superalloys have replaced austenitic stainless steels for use in components of various industrial boilers and incinerators that operate at high temperature under corrosive conditions.

Recently, several industrial plants began using a new type of burner, the so-called low NOx burner, which operates at higher temperatures than conventional units. This new design has replaced austenitic stainless steels with Ni-Co-Cr-base alloys for the metallic components in order to withstand the high temperatures and corrosiveness of the fuel-rich zone. Such alloys are useful due to their combination of good high-temperature strength, thermal stability, and high-temperature corrosion resistance to environments containing sulfur and chlorides. Moreover, their excellent room-temperature ductility provides superior fabricability.

Welding of this type of alloy, however, poses the same types of problems as those frequently encountered in the welding of austenitic stainless steels—for example, solidification cracking and microfissuring (Ref 1-3). The controlling factors for solidification cracking are the chemical composition of the filler metals and the welding parameters. The solidification cracking of weldments has been successfully avoided by selecting filler metals with a lower content of detrimental elements, such as phosphorus and sulfur, and by employing low heat input and interpass temperature in the welding process (Ref 1-7).

Another important issue in the welding of Ni-Co-Cr-base alloys is degradation of mechanical properties, such as a drastic decrease of weld ductility in the as-welded condition (Ref 1). Poor ductility has been attributed to the formation of a second phase with a low melting temperature. These second phases, which are strongly affected by the segregation of alloying elements, can possibly be minimized by postweld heat treatment (PWHT) (Ref 1).

This study investigates the effects of PWHT on the properties of gas tungsten arc (GTA) weldments of a commercial wrought Ni-Co-Cr-base alloy, focusing on the subsequent improvement in the mechanical properties of the weldments. An optimum PWHT is proposed for application to the actual fabrication procedure.

C.-S. Lim and **K.-K. Baek,** Hyundai Industrial Research Institute, Hyundai Heavy Industries Co., Ltd., 1 Jeonha-Dong, Ulsan, Korea 682-792.

2. Experimental Procedure

2.1 *Materials*

The nominal chemical compositions of the alloy and filler metal are given in Table 1. Plate thickness was 6.4 mm for the U-bend and tensile tests, and 12.7 mm for the all-weld-metal tensile test. Matching filler metals were 2.4 mm diam straight wire.

Table 1 Chemical composition of base metal and filler metal

	Composition, wt%									
Material	Ni	Co	Cr	Si	Mn	Ti	Fe	C	S	P
Base metal	41.1	28.4	26.4	2.82	0.82	0.47	0.10	0.06	0.001	0.002
Filler metal	39.4	28.7	27.5	2.81	0.71	0.49	0.10	0.06	0.001	0.002

2.2 *Welding and Postweld Heat Treatment*

Several batches of GTA weldments with different heat input were prepared. Microstructural examination of the weldments confirmed the absence of both fusion-zone solidification cracking and microfissuring. Welding parameters are summarized in Table 2. U-bend and tensile specimens were prepared by one-side flat-position welding with a 60° single-V groove design and a 4 mm root gap. All-weld-metal specimens had a 20° single-V groove design and a 12 mm root gap with a backing plate.

Heat treatment was carried out in a box furnace, where the temperature of the specimen surface was monitored by an attached K-type thermocouple. Postweld heat treatments were conducted at a holding temperature in the range of 880 to 1095 °C, followed by air cooling.

2.3 *Mechanical Testing*

Mechanical property evaluation included U-bend and transverse tensile testing. Before the weldments were machined to the final specimen configuration, they were heat treated under specific PWHT conditions. A universal tensile tester with a 100 ton capacity and a 2T guided bend tester (bending radius two times the plate thickness) were used.

2.4 *Microstructural Evaluation*

Representative weldment samples containing weld metal as well as the heat-affected zone immediately adjacent to the fusion line were metallographically prepared to characterize microstructural features. The specimens were polished using 0.05 μm alumina and electroetched in a solution of 60 mL HCl, 35 mL HNO_3, and 25 mL methanol at 10 to 15 V. Optical microscopy was used to examine the specimens at magnifications up to 500×. Several specimens were also examined at higher magnifications using a scanning electron microscope (SEM) equipped with an energy-dispersive spectrometer (EDS). The SEM was also used to examine the fracture surfaces of tensile and U-bend test specimens. An electron probe microanalyzer (EPMA) was used for chemical analysis of different phases found in the SEM observations.

Table 2 GTA welding parameters

Parameter	Value
Current, A	115-140
Voltage, V	10-12
Heat input, kJ/cm	8.9-11.2
Travel speed, cm/min	4.7-10.5
Argon shielding gas rate, L/min	15
Interpass temperature, °C	<90

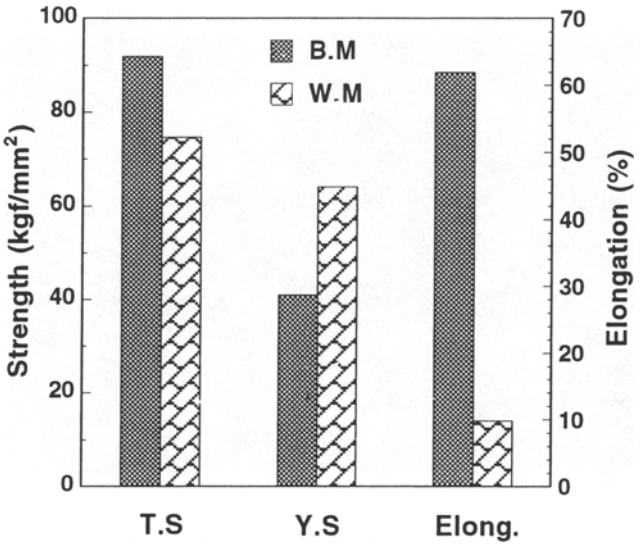

Fig. 1 Tensile properties of weld metal and base metal

3. Results and Discussion

3.1 *Mechanical Properties*

Results of tensile and U-bend tests on the as-welded GTA weldments with no solidification cracking are summarized in Table 3. All tensile test specimens fractured at weld metal, and bend testing yielded overall cracks in the weld metal regardless of welding heat input. Figure 1 compares the tensile properties of the all-weld-metal deposits with those of solution-annealed base metal. The tensile elongation was only 9% in the as-welded condition, whereas a fully solution-annealed alloy showed an elongation of 62%, which suggests very brittle weld metal in the as-welded condition.

Table 3 Mechanical properties of as-welded GTA weldments at room temperature

Thickness, mm	Tensile strength, kgf/mm²(a)	Location of rupture	2T guided bend test(b)	
6.4	74.4	Weld metal	Face	Cracked
			Root	No crack
12.7	69.4	Weld metal	Side	Cracked

(a) ASME SFA-5.11 (25.4 mm gage length, 6.4 mm diam) for transverse tensile test. (b) ASME QW-462 (38 × 240 × 6.4 mm)

Fig. 2 Fracture surface of U-bend test specimens

In an attempt to increase the ductility of the weld metal, various welding heat inputs were applied. It has been reported (Ref 8, 9) that lower heat input, as used in the present study, results in faster solidification of the weld pool, which would suppress segregation of the alloying elements due to narrower interdendritic spacing. However, the mechanical test results of the various welds with different heat inputs (Table 4) indicated that the weld metal still lacked proper ductility, exhibiting cracks at the weld metal during U-bend testing. This suggests that controlling welding parameters alone cannot improve weld metal ductility in the as-welded condition.

3.2 *Microstructural Analysis*

The fracture surface of a U-bend test specimen in the as-welded condition is shown in Fig. 2. A continuous, filmlike second phase at the dendrite interface is mixed with a dimple-type fracture surface.

Metallographic evaluation of this interdendritic second phase was carried out on overetched, cross-sectional weld metal. Scanning electron micrographs of the overetched weld metal microstructure (Fig. 3a, b) showed a very aggressive wetting action of the liquid phase. Figure 3(b), a magnified view of the weld metal, reveals that the weld metal was characterized by a series of continuous eutectic phases with considerable liquation of the phase along with interdendritic boundaries. Analysis of the matrix and the continuous eutectic phase by

Table 4 Bend Test Results with Various Heat Input

Type	Heat input (kJ/cm)	Travel speed (cm/min)	Interpass temp. (°C)	2T guided bend test
Low heat input	5.0	13.4	<90	Cracking
Normal	8.9	10.5	<20	Cracking
High heat input	11.2	7.3	<185	Cracking

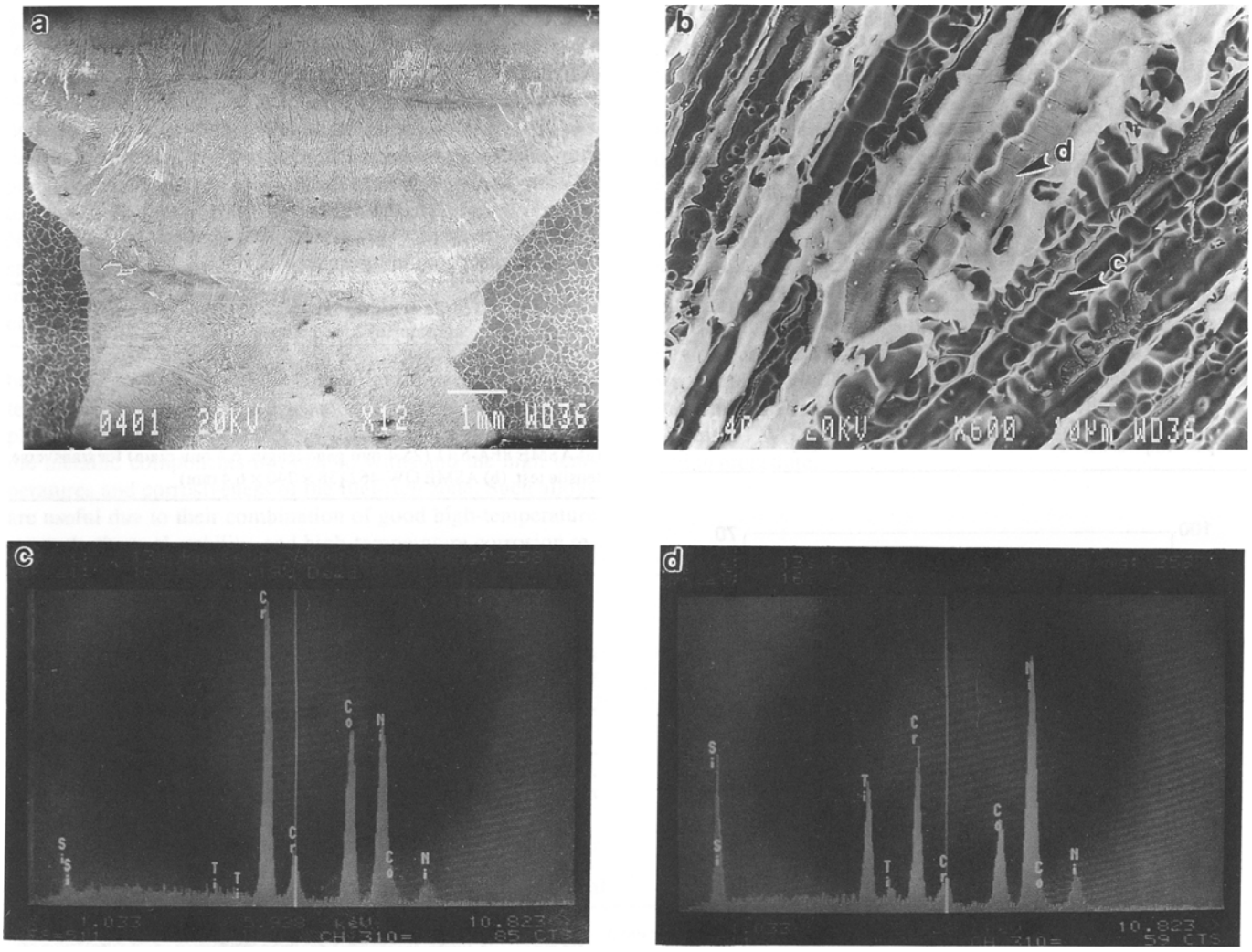

Fig. 3 (a) and (b) SEM micrographs of the overetched weld metal microstructure. (c) EDS results for the matrix. (d) EDS results for the continuous eutectic phase

EDS (Fig. 3c, d, respectively) strongly suggested that the eutectic phase consisted primarily of $(Si,Ti)_xNi_y$.

Analysis of the eutectic phase by EPMA (Fig. 4) confirmed the EDS observation that the eutectic phase was enriched with silicon, titanium, nickel, and carbon, as well as being depleted of chromium and cobalt. Therefore, the rather brittle nature of the Ni-Co-Cr-base weld metal in the as-welded condition appears to have originated through the formation of an interdendritic eutectic phase of low melting temperature during solidification of the weld pool.

This type of eutectic phase with a liquid filmlike nature can also promote solidification cracking or microfissuring in the weld metal under highly stressed conditions (Ref 10). Interdendritic microfissures approximately 30 to 80 μm in length were observed in the weldments with high heat input i this study. Figure 5 shows microfissuring in the reheated zone of the high-heat-input weld, where the eutectic phase provided constitutional liquation reaction between the carbide and the matrix (Ref 4, 8, 10).

3.3 *Postweld Heat Treatment*

Based on reports that PWHT would enhance the ductility of the alloy weldments, proper conditions for PWHT were evaluated by varying the holding temperature and time. To select the optimum range of PWHT temperature, previously reported transformation temperatures were reviewed. The solution annealing temperature of the Ni-Co-Cr-base alloy was 1105 °C, whereas binary phase diagrams of Ni-Si and Ni-Ti suggested eutectic temperature of 1152 and 942 °C, respectively (Ref 11). Differential thermal analysis (DTA) of the weld deposit, carried out previously by the authors, indicated the melting temperature of the eutectic phase to be in the range of 940 to 1058 °C (Ref 12).

These evaluations led to PWHT temperatures in the range of 880 to 1095 °C for the weldments. Figure 6 compares the tensile properties of all-weld-metal deposits before and after PWHT of 1095 °C for 1 h, followed by air cooling. The PWHT increased the room-temperature elongation of the weld metal from a value of 9% to about 44%. Figure 6 also indicates that PWHT caused an increase in weld tensile strength as well as a decrease in yield strength.

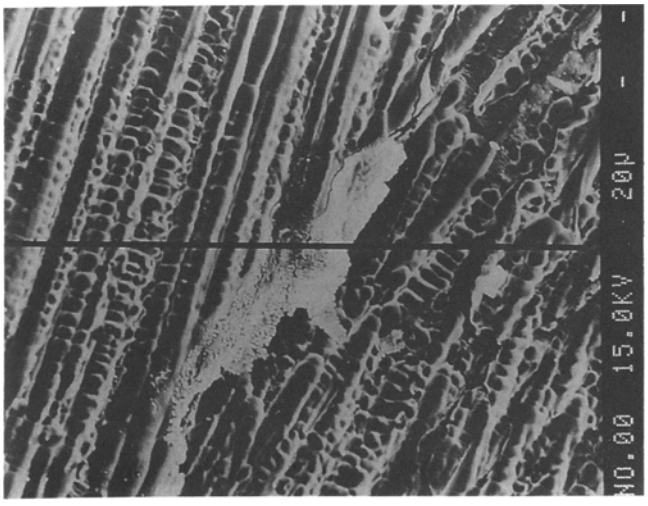

(a)

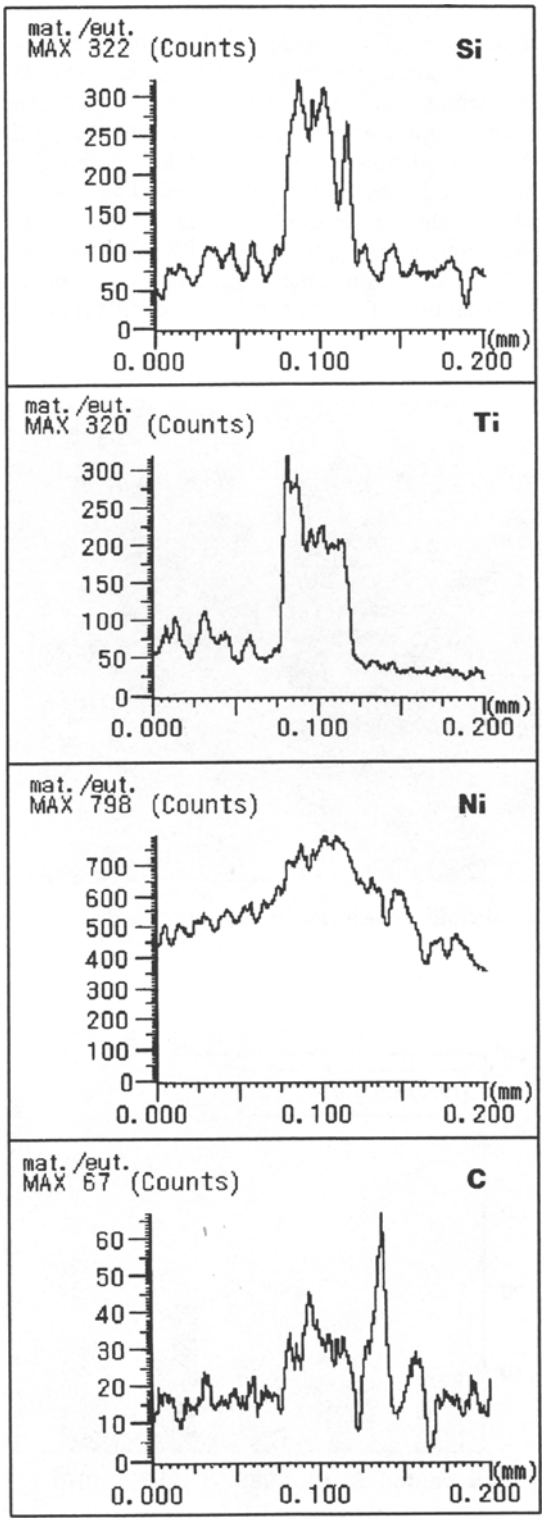

(b)

Fig. 4 (a) SEM micrograph of the overetched weld metal microstructure. (b) EPMA results of line scanning of the eutectic phase

A series of PWHTs were also conducted for 1 h at various holding temperatures in the range of 880 to 1095 °C, and subsequent room-temperature elongation results are plotted in Fig. 7. Elongation of the weld after PWHT was found to increase with PWHT temperature. An especially sharp increase in elongation after PWHT above 985 °C is quite noticeable.

Bend test results for all-weld-metal specimens subjected to various PWHT conditions are plotted in Fig. 8, which indicates that higher temperature and longer time results in sounder weld metal with no cracking. Temperatures greater than 1200 °C should be avoided, however, because of the possibility of base material grain growth and incipient melting. The melting range of the alloy is about 1226 to 1303 °C, as determined by DTA. The lower temperature limit for the PWHT "window" was about 985 °C, below which the longer holding time did not improve weld ductility. Therefore, the optimum PWHT condition for the alloy welds is 1050 °C for 1 h, followed by air cooling, which enables the welds to pass the 2T guided bends test.

Microstructurally, the effect of PWHT is to break up the continuous network of eutectic phase in the weld metal. Scanning electron micrographs of the overetched weld metal before and after PWHT (Fig. 9) confirm this explanation. The continuous network of eutectic phase found in the weld metal in the as-welded condition was drastically reduced after PWHT at 1095 °C for 1 h. On the other hand, a series of smaller carbides ($M_{23}C_6$) formed along the interdendrite boundaries during the rather slow air-cooling process (Ref 1).

Fractographs of the tensile test specimens before and after PWHT revealed the same phenomenon (Fig. 10). The fracture surface of the as-welded specimen (Fig. 10a) revealed a very aggressive wetting action of the liquid phase, whereas a much smaller quantity of the liquid phase was visible in the fracture surface of the specimen subjected to PWHT at 1095 °C (Fig. 10d).

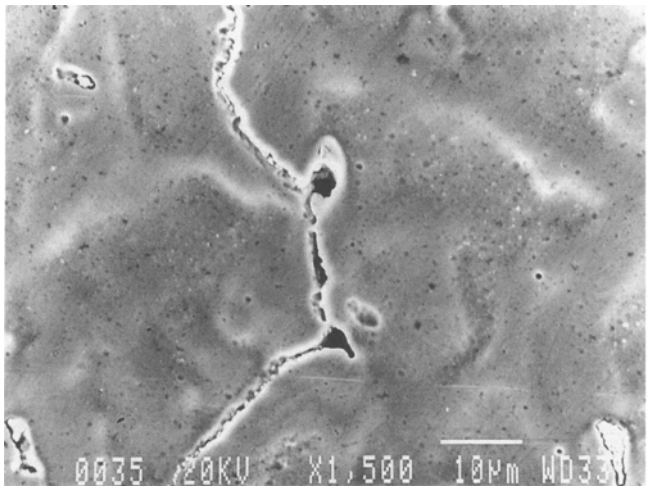

Fig. 5 Microfissuring in interpass region of weld metal

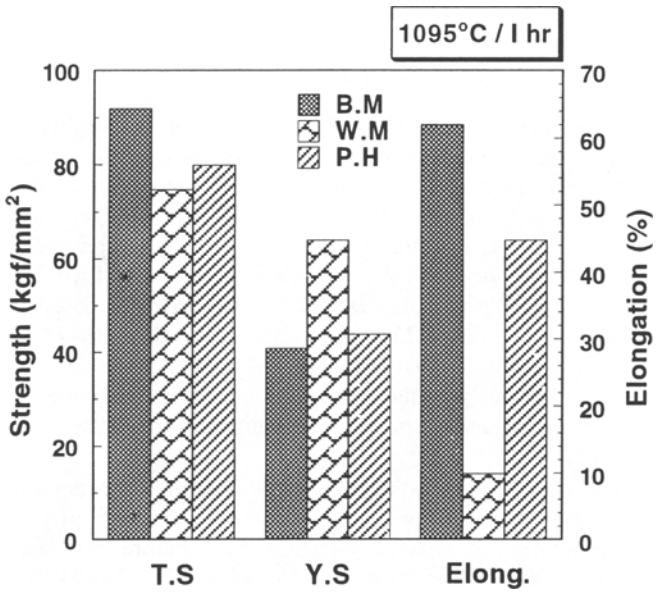

Fig. 6 Tensile properties of as-welded and PWHT specimens

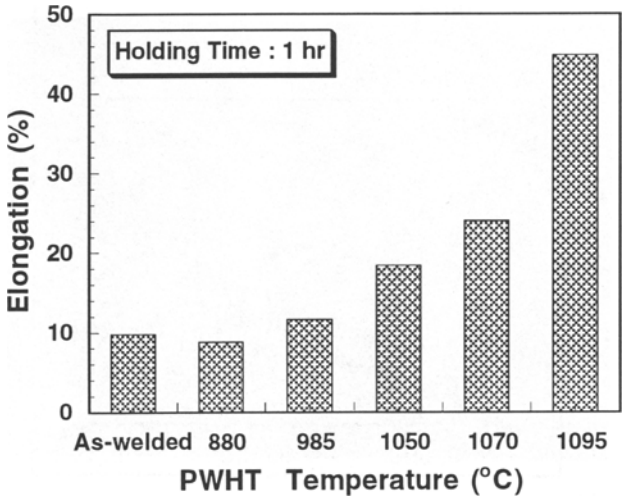

Fig. 7 Ductility change for various PWHT temperatures (all-weld-metal tensile test)

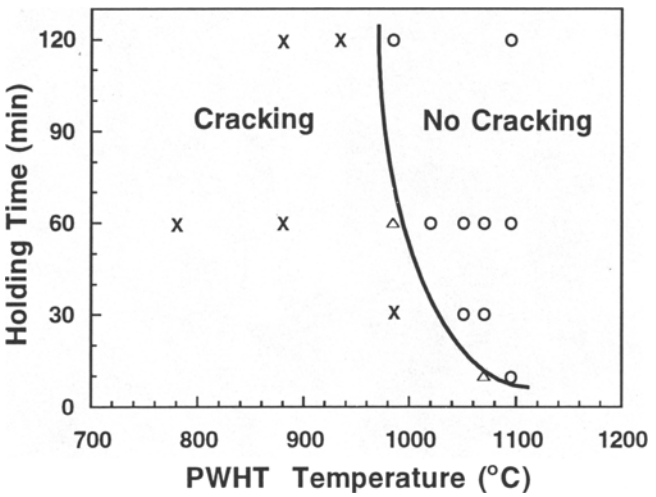

Fig. 8 2T guided bend test results for various PWHT conditions

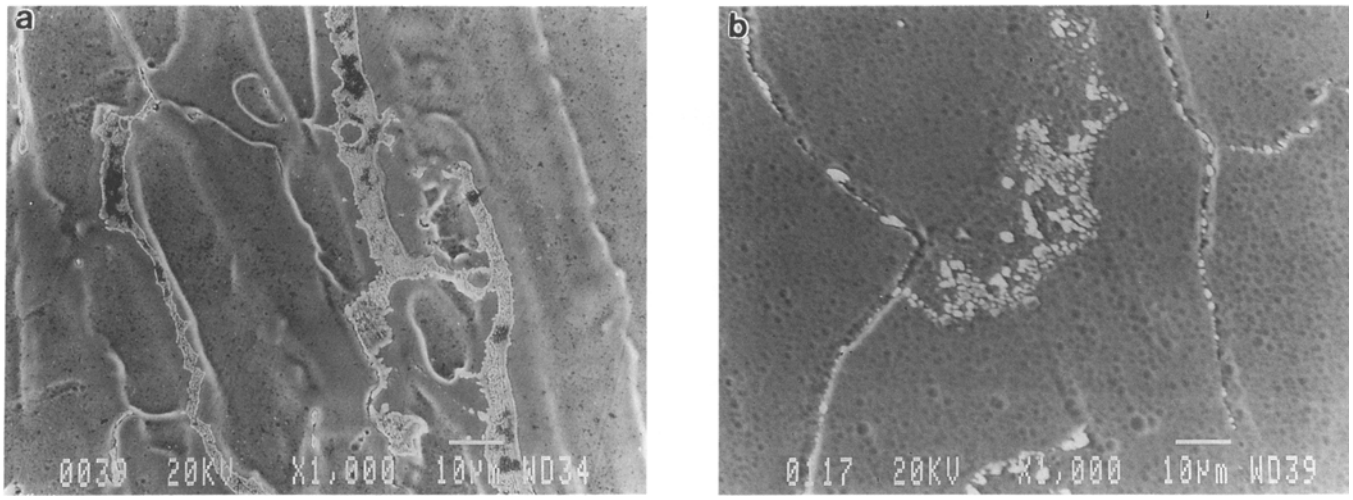

Fig. 9 SEM micrographs of weld metal. (a) As welded. (b) After PWHT

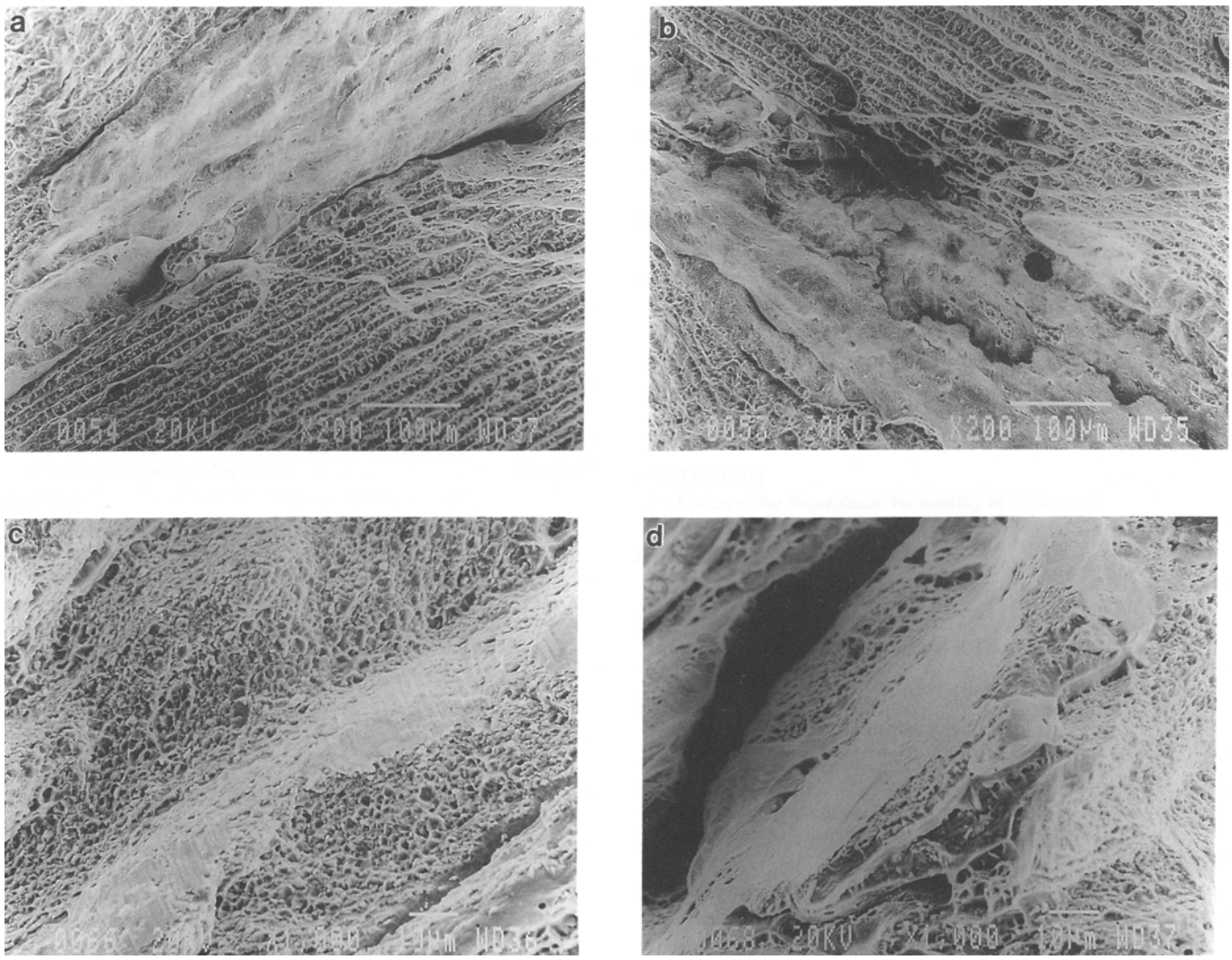

Fig. 10 Fracture surfaces of all-weld-metal tensile specimens. (a) and (b) As welded. (c) and (d) After PWHT

4. Conclusions

- The welding characteristics of a wrought nickel-base alloy with a nominal composition of Ni-28Cr-29Co-2.75Si-0.5Ti revealed mechanical property limitations of the alloy weld metal in the as-welded condition.
- Poor weld ductility in the as-welded condition caused by a continuous eutectic phase, consisting primarily of $(Si,Ti)_xNi_y$, was successfully reduced or eliminated by proper PWHT.
- Alloy PWHT is necessary if cold forming is required after welding or if adequate joint ductility is a design requirement. The recommended PWHT temperature is 1050 °C for 1 h, followed by air cooling.

References

1. W. Yeniscavich, Joining, *Superalloys II*, C.T. Sims, N.S. Stoloff, and W.C. Hagel, Ed., John Wiley & Sons, 1987, p 495-516
2. C.D. Lundin, C.-P. Chou, and C.J. Sullivan, Hot Cracking Resistance of Austenitic Stainless Steel Weld Metals, *Weld. J.*, Vol 59 (No. 8), 1980, p 226s-232s
3. W.F. Savage and B.M. Krantz, Microsegregation in Autogenous Hastelloy X Welds, *Weld. J.*, Vol 50 (No. 7), 1971, p 292s-303s
4. G.E. Linnert, *Weldability of Austenitic Stainless Steel as Affected by Residual Elements*, STP 418, ASTM, 1967, p 105-119
5. T.G. Gooch and J. Honeycombe, Welding Variables and Microfissuring in Austenitic Stainless Steel Weld Metal, *Weld. J.*, Vol 59 (No. 8), 1980, p 233s-241s
6. J.C. Lippold and W.F. Savage, Solidification of Austenitic Stainless Weldments, Part III: The Effect of Solidification Behavior on Hot Cracking Susceptibility, *Weld. J.*, Vol 61 (No. 12), 1982, p 388s-396s
7. R.P. George, The Practical Welding Metallurgy of Nickel and High-Nickel Alloys, *Weld. J.*, Vol 36 (No. 7), 1957, p 330s-334s
8. K. Eastering, *Welding Metallurgy*, John Wiley & Sons, 1989, p 89
9. J.C. Boland, Generalized Theory of Super-Solidus Cracking in Weld (and Castings), *B. Weld. J.*, Aug 1960, p 508-512
10. S.C. Ernst, Weldability Studies of Haynes 230 Alloys, *Weld. J.*, Vol 73 (No. 4), 1994, p 80s-86s
11. E.N. Skinner, Ni-Si Equilibrium Diagram, *Smithells Metals Reference Book*, 7th ed., E.A. Brandes and G.B. Brook, Ed., McGraw-Hill, 1992, p 405
12. C.-S. Lim and K.-K. Baek, unpublished study